Quantification of Focal Outflow Enhancement Using Differential Canalograms

Ralitsa T. Loewen,[1] Eric N. Brown,[2] Gordon Scott,[1] Hardik Parikh,[1,3] Joel S. Schuman,[1,4] and Nils A. Loewen[1]

[1]Department of Ophthalmology, University of Pittsburgh Medical Center, Pittsburgh, Pennsylvania, United States
[2]Department of Ophthalmology, Vanderbilt University School of Medicine, Nashville, Tennessee, United States
[3]School of Medicine, Rutgers State University of New Jersey, New Brunswick, New Jersey, United States
[4]School of Medicine, New York University, New York, New York, United States

Correspondence: Nils A. Loewen, Department of Ophthalmology, University of Pittsburgh, 203 Lothrop, Suite 819, Pittsburgh, PA 15213, USA;
loewen.nils@gmail.com.

Submitted: March 10, 2016
Accepted: April 23, 2016

Citation: Loewen RT, Brown EN, Scott G, Parikh H, Schuman JS, Loewen NA. Quantification of focal outflow enhancement using differential canalograms. *Invest Ophthalmol Vis Sci.* 2016;57:2831–2838. DOI:10.1167/iovs.16-19541

Purpose. To quantify regional changes of conventional outflow caused by ab interno trabeculectomy (AIT).

Methods. Gonioscopic, plasma-mediated AIT was established in enucleated pig eyes. We developed a program to automatically quantify outflow changes (R, package eye-canalogram, github.com) using a fluorescent tracer reperfusion technique. Trabecular meshwork (TM) ablation was demonstrated with fluorescent spheres in six eyes before formal outflow quantification with two-dye reperfusion canalograms in six additional eyes. Eyes were perfused with a central, intracameral needle at 15 mm Hg. Canalograms and histology were correlated for each eye.

Results. The pig eye provided a model with high similarity to AIT in human patients. Histology indicated ablation of TM and unroofing of most Schlemm's canal segments. Spheres highlighted additional circumferential and radial outflow beyond the immediate area of ablation. Differential canalograms showed that AIT caused an increase of outflow of 17 ± 5-fold inferonasally, 14 ± 3-fold superonasally, and also an increase in the opposite quadrants with a 2 ± 1-fold increase superotemporally, and 3 ± 3 inferotemporally. Perilimbal specific flow image analysis showed an accelerated nasal filling with an additional perilimbal flow direction into adjacent quadrants.

Conclusions. A quantitative, differential canalography technique was developed that allows us to quantify supraphysiological outflow enhancement by AIT.

Keywords: canalogram, porcine eyes, trabecular meshwork, glaucoma, segmental outflow

Bulk outflow of aqueous humor and its relationship to intraocular pressure (IOP) has been well characterized.[1,2] In contrast, focal outflow and enhancement of focal outflow by microincisional glaucoma surgeries has only been modeled mathematically,[3,4] but not measured directly. Tracers have been used to highlight areas of increased flow through the trabecular meshwork (TM) where they become lodged near collector channel openings.[5,6] The trabecular meshwork and the aqueous spaces of Schlemm's canal and collector channels in the superficial to midlevel sclera can also be imaged noninvasively by spectral-domain optical coherence tomography (SD-OCT).[7] Wang et al.[8] used a Doppler strategy to detect movements of gold nanorods by SD-OCT but a quantification of flow could not be obtained. This approach may have limited use in vivo due to toxicity.[9]

It is estimated that the smallest of the current trabecular meshwork microbypass implants is limited to drainage segments of about 60°,[10,11] while larger ones access additional clock hours.[12] Trabecular meshwork ablation can provide more extensive angle access by allowing areas of discontinuity of the Schlemm's canal (SC) to be skipped (bypassed).[11,13] Although the trabecular meshwork is thought to be the anatomic location of primary outflow resistance,[14] intraocular pressures that are close to the theoretical limit of episcleral venous pressure[11] are rarely achieved with trabecular bypasses[15] or with trabecular ablation.[16]

Here, we hypothesized that it is possible to develop a differential canalography technique to directly analyze areas of altered outflow before and after an intervention. We refined recently introduced methods of quantitative canalography[17] and used them to measure conventional outflow enhancement following plasma-mediated ab interno trabeculectomy (AIT). We also present here the first animal model for AIT that provides tissues fresh enough to allow direct gonioscopic visualization[11] of the large, wedge-shaped TM. It guards outflow into the circumferential drainage segments of the characteristic angular aqueous plexus,[18] a structure that is relatively analogous to the Schlemm's canal in primates.[19] Another feature that is relevant to glaucoma research is that the porcine genome is a close match to the human genome[20–22] and the anterior segments show biochemical glaucoma markers[19] and giant vacuole formation similar to human eyes.[23]

Methods

Trabectome-Mediated AIT in Pig Eyes

Pig eyes were obtained from a local abattoir. Only eyes that could be identified as right eyes were used. Within 2 hours of death, eyelids and adnexal structures were excised. The bulbar

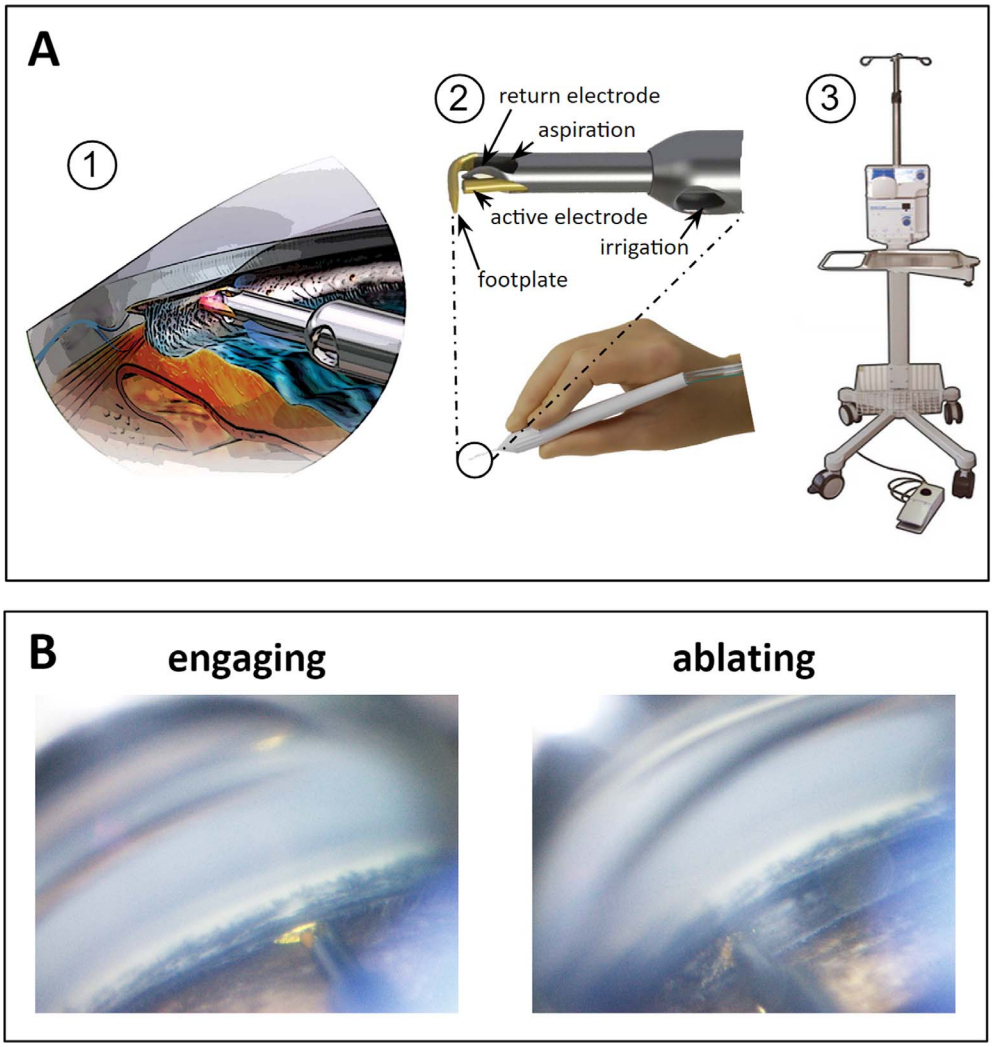

Figure 1. Trabectome-mediated AIT in porcine eyes. (**A**) (**1**) Trabectome inserted through a clear corneal incision ablates TM that is engaged in between footplate and bipolar electrodes. (**2**) Handpiece and magnified view of tip. (**3**) Stand, operating console with peristaltic pump and high frequency generator and footswitch. (**B**) Direct, gonioscopic view of ablation in porcine eye immediately before engaging the TM (*left*) and with tip obscured by TM during ablation (*right*).

conjunctiva was preserved, while the palpebral conjunctiva was removed together with adnexal tissues. Eyes irrigated with PBS were placed with the optic nerve into a cryogenic vial cup (CryoElite cryogenic vial #W985100; Wheaton Science Products, Millville, NJ, USA) for compression free mount as described before.[17] Similar to AIT in human eyes (Fig. 1A),[11] eyes were positioned under a surgical microscope looking up with the temporal side of the eye directed toward the surgeon. A clear corneal incision was fashioned with a 1.8-mm keratome approximately 2 mm anterior to the temporal limbus while the inside was slightly flared for a striae-free visualization during the procedure. Eyes were then tilted 30° away from the surgeon and a goniolens (Trabectome Goniolens ONT-L, #600010; Neomedix, Inc., Tustin, CA, USA) was placed on the cornea to visualize the chamber angle (Fig. 1B). The tip of a microsurgical handpiece (#600018; Neomedix, Inc.) that was connected to a standard microsurgical system (Trabectome System #600026; Neomedix, Inc.) was inserted and advanced to the opposite nasal angle of the anterior chamber. Since only right eyes were used in this study, this would represent the anatomic 3 o'clock position. After gentle goniosynechiolysis with the side of the instrument's tip to disengage pectinate ligaments along the nasal angle,[24] TM ablation (Fig. 2 with insert) was continued toward the left by 45°. The tip was then turned around inside of the eye, the TM was engaged again, and ablation continued by 45° in the opposite direction. The instrument was withdrawn and the incision sealed with a drop of cyanoacrylate.

Microsphere Canalograms

Fluorescent microsphere canalograms were obtained in six eyes after AIT. In pilot experiments, microspheres were tested for a size that is known to not pass through human TM within the perfusion time used here[6] (Fig. 3A) while allowing visualization of the collector channels after the TM was removed (Fig. 3B). We chose 0.5 μm diameter carboxylate-modified microspheres (FluoSpheres, 0.5 μm, yellow-green fluorescent [505/515], 2% solids; Thermo Fisher Scientific, Eugene, OR, USA). The fluorescent microspheres were diluted 100-fold with phenol red free Dulbecco's modified Eagle's media (DMEM) to make the perfusate. Following the intervention described below, AIT, a 30-gauge needle was inserted through the nasal cornea 2 mm anterior to the limbus with the tip of the needle positioned in the center of the anterior chamber. The head (fluid meniscus) was positioned at 204 mm height above the needle, the equivalent of 15 mm Hg, and the stopcock was opened to start the gravity-

Investigative Ophthalmology & Visual Science

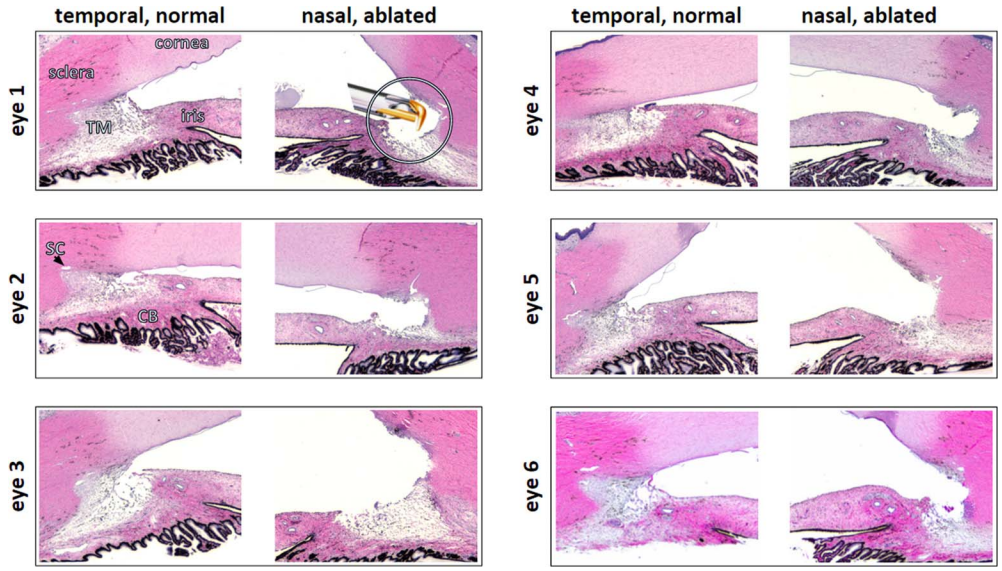

Figure 2. Histology of ablated, nasal TM and normal, temporal TM. Eye numbers match eyes in other figures throughout manuscript. *Insert*: trabectome tip shown to scale.

based infusion. Fluorescence was visualized with a stereo dissecting microscope equipped for fluorescent imaging (Olympus SZX16 with GFP filter cube and DP80 monochrome/color camera; Olympus Corp., Center Valley, PA, USA). Images during time lapse analysis (CellSens; Olympus Life Science, Tokyo, Japan) were acquired every 20 seconds for 15 minutes using 2 × 2 pixel binning and a resulting resolution of 580 × 610 pixels. To better obtain a contiguous image of the microbead distribution, whole eyes were processed as previously described.[17,25] Briefly, after removing all adnexal structures, globes were hemisected

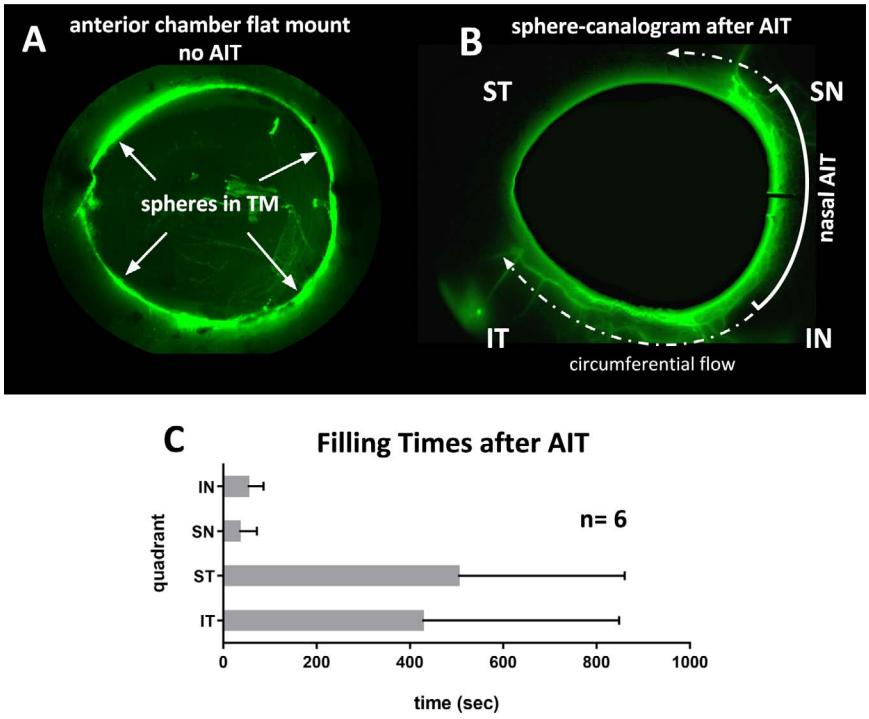

Figure 3. Microsphere canalograms pre- and post-AIT. (**A**) Perfusion of eye with fluorescent microspheres that cannot pass through the TM in a control eye (*top left*, inside view after removal of uvea and iris), but light up the nasal outflow tract. There is additional flow beyond the ablation ends along the circumferential drainage elements and away from the eye along collector channels (*dashed arrow*). (**B**) Preferentially nasal outflow system filling is observed (anterior chamber subtracted using baseline). Circumferential filling can be seen (see Supplementary Movie S1). (**C**) Short filling times after AIT nasal quadrants with occasional flow into adjacent quadrants. Filling times of ST and IT quadrants without nonfilling eyes was 67 ± 22 seconds and 46 ± 29 seconds, respectively.

Investigative Ophthalmology & Visual Science

along the equator. Subsequently, the entire uvea, including ciliary body (CB) and iris, was gently detached and the anterior segment was inspected with the dissecting microscope detailed above.

Differential Canalograms

A fluorescent tracer reperfusion technique was used in six eyes to compare outflow changes before and after AIT detailed below using a quantitative canalography method we recently developed.[17] Reperfusion canalograms to analyze results of trabecular ablation required two different water soluble dyes because of partial diffusion into the extravascular space over time that makes displacement or washout attempts incomplete. Use of colloids (more viscous solutions) would have changed the canalogram dye flow behavior and made it less similar to that of aqueous humor. We selected two fluorescent dyes that can be readily detected with common fluorescent filter cubes used in epifluorescent microscopes and have a reasonably low toxicity to be useful in future in vivo experimentation, fluorescein and Texas red.[26] Both are displayed in monochromatic green throughout this manuscript for easier comparison.

Whole pig eyes were prepared and mounted under a surgical microscope as previously described. A 30-gauge needle was inserted through the nasal cornea as previously described and used to remove 0.2 mL of anterior aqueous humor from the whole eye's anterior segment. A 30-gauge needle was then placed in the anterior segment using the exact same entry site and media with fluorescein (AK-FLUOR 10%, fluorescein injection, USP, 100 mg/mL, NDC 17478-253-10; Akorn, Lake Forest, IL, USA), at a concentration of 0.017 mg/mL, was infused via gravity. The outflow pattern was imaged every 20 seconds for 15 minutes using a stereo dissecting microscope equipped for fluorescent imaging (Fig. 4). Fluorescein flow was then stopped and the needle was removed. Following AIT, a new 30-gauge needle was placed in the anterior segment using the same entrance wound, and media with 0.28 mg/mL Texas red (sulforhodamine 101 acid chloride, 10 mg; Alfa Aesar, Ward Hill, MA, USA) was subsequently infused via gravity. Again the outflow pattern was imaged every 20 seconds for 15 minutes. The eyes were then fixed and sent for histology.

To determine differences in chromophore detection sensitivity, a hemocytometer chamber was filled with 10 μL each of fluorescein and Texas red at the previously stated concentrations. Proper exposure times of 15 ms for fluorescein and 10 ms for Texas red were determined with the fluorescence equipped stereo dissecting microscope above.

Initially, six eyes were perfused with fluorescein first immediately followed by Texas red without AIT. Another six eyes were perfused with Texas red first followed by fluorescein to determine whether the order of perfusion would have any effect. We chose the order to be fluorescein followed by Texas red to avoid a type I error (false positive flow enhancement) because Texas red had a slightly slower filling average that was not statistically significant in pilot eyes ($P = 0.06$, $n = 12$).

Quantification of Outflow Change

As described before,[17] we used a program written in R[27] to automatically compute the focal outflow changes (Fig. 5, left) and convergent perilimbal aqueous flow (Fig. 5, right) using the eye-canalogram package to process the image datasets, the source code of which we made available for download (R package "eye-canalogram," provided in the public domain at https://github.com/enbrown/eye-canalogram/tree/06461498c8).

Briefly, for each image set, the cornea was first manually delineated and masked to exclude the bright fluorescence in the anterior chamber from the image analysis. This step was neutral to the mathematical analysis of fluorescence changes along the outflow tract but considerably improved how observers were able to see and interpret subtle filling of small caliber vessels (Fig. 4).

The image resolution was then reduced to 32 × 32 macropixels per image. Generalized additive models (GAM) were fit for each macropixel. Metrics from the fit were recorded and graphically displayed (Supplementary Fig. S1). In dot plot images, larger pixels corresponded to more intense fluorescein signals while red dots corresponded to faster flow.

In addition, all regions (clock hour and three radial rings) were fit to a single GAM using smoothing terms for the radial ring, clock hour, and frame number. Pre- and posttreatment image sets for each eye were registered using the clock hour and radial distance to compute the change in fit metrics (Fig. 6A). Similarly, all eyes were warped to a common reference frame and averaged to produce Figure 6B.

Each quadrant was also analyzed for first detection of fluorescence in an outflow structure downstream of Schlemm's canal segments. Timestamps from time-lapse recordings were summarized as graphs (average ± SD) for the inferonasal (IN), superonasal (SN), superotemporal (ST), and inferotemporal (IT) quadrants. Student's paired two sample *t*-test was used to compare outflow changes in the same eyes before and after each intervention and to compare same eye quadrants. Tests were two-tailed and results were reported as mean ± SD.

Histology

Segments were removed from the perfusion dish, rinsed in PBS, cut into quarters, and fixed with 4% paraformaldehyde and PBS for 48 hours before being placed in 70% ethanol. A corneoscleral wedge was taken from the lateral side near the incision and one from the nasal side where the AIT had been performed (Fig. 2). The section was paraffin-embedded for histological processing, cut at 6-μm thickness, and stained with hematoxylin and eosin.

Results

Visualization and TM ablation could be achieved with a standard microsurgical system (Neomedix, Inc.) and the kit included, modified Swan Jacob goniolens (Fig. 1A). Pectinate ligaments had to be gently lysed (Fig. 1B, left) before the TM could be engaged for ablation (Fig. 1B, right). Power and aspiration settings were identical to surgery in human patients. During ablation, the footplate encountered more stops than typical for human eyes when SC segment ends were reached.

The histologic analysis showed that the relatively prominent TM and common SC segments had been ablated with a few exceptions of SC segments too small to enter with the trabectome tip (Fig. 2, eye 1, shown to scale). No coagulative damage was observed.

Eyes without AIT that were infused with fluorescent spheres showed fluorescence only in the TM. When those were hemisected and the vitreous and iris removed, sphere distribution appeared relatively even throughout the TM circumference (Fig. 3A). In contrast, canalograms with fluorescent spheres obtained after AIT experienced fast filling of proximal and distal parts of the outflow system along the ablation site followed by circumferential and then centrifugal filling of adjacent quadrants. Filing of nasal quadrants was nearly 10 times faster than that of temporal quadrants (Fig. 3B).

Differential canalograms, obtained before and after AIT (Fig. 4 and Supplementary Movie S1) had a 17 ± 5-fold increase in

Investigative Ophthalmology & Visual Science

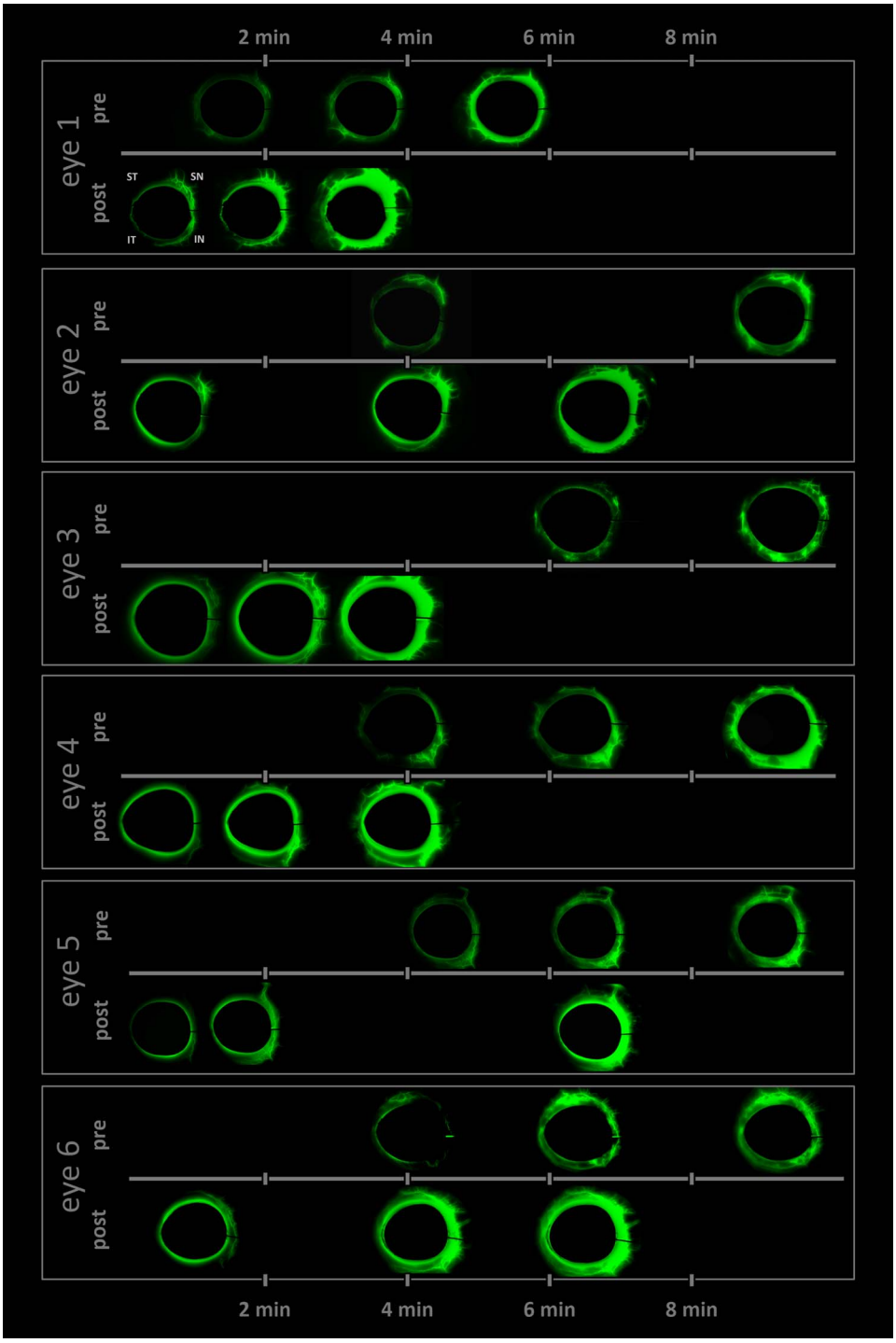

Figure 4. Time lapse of differential canalograms for each eye. Images are subtracted from baseline to suppress nonspecific fluorescence. Frames selected show filling of new segments. Pre- and post-AIT canalogram frames are matched (also see Supplementary Movie S1).

filling IN, 14 ± 3-fold increase SN, and also an increase in the adjacent quadrants, with a 2 ± 1-fold increase ST and 3 ± 3 IT. The superonasal quadrant was the fastest to fill ($P < 0.05$) followed by the IN, ST, and IT quadrants (Figs. 4, 7). Although fluorescent dyes used in these differential canalograms were not blocked by the TM like the fluorescent spheres, ST and IT quadrants often filled circumferentially from the site of AIT.

Individual fit curve analysis indicated a shift in filling speed toward the nasal side and an overall faster filling throughout the remainder of the outflow system in most eyes (Fig. 5). This can be seen by a shift toward red in the color coded analysis indicating a shorter time toward peak fluorescence, as well as the increased bubble size that describes the peak fluorescence obtained. When perilimbal flow was examined specifically, circumferential filling was evident. With the exception of eye 1, all eyes post-AIT showed an initial uptake centered on the IN and SN quadrants as expressed by the red color coding that spreads circumferentially from here (Fig. 5).

Changes from pre- to post-AIT fluorescence intensity changes are summarized in Figure 6. In average of all six eyes,

Investigative Ophthalmology & Visual Science

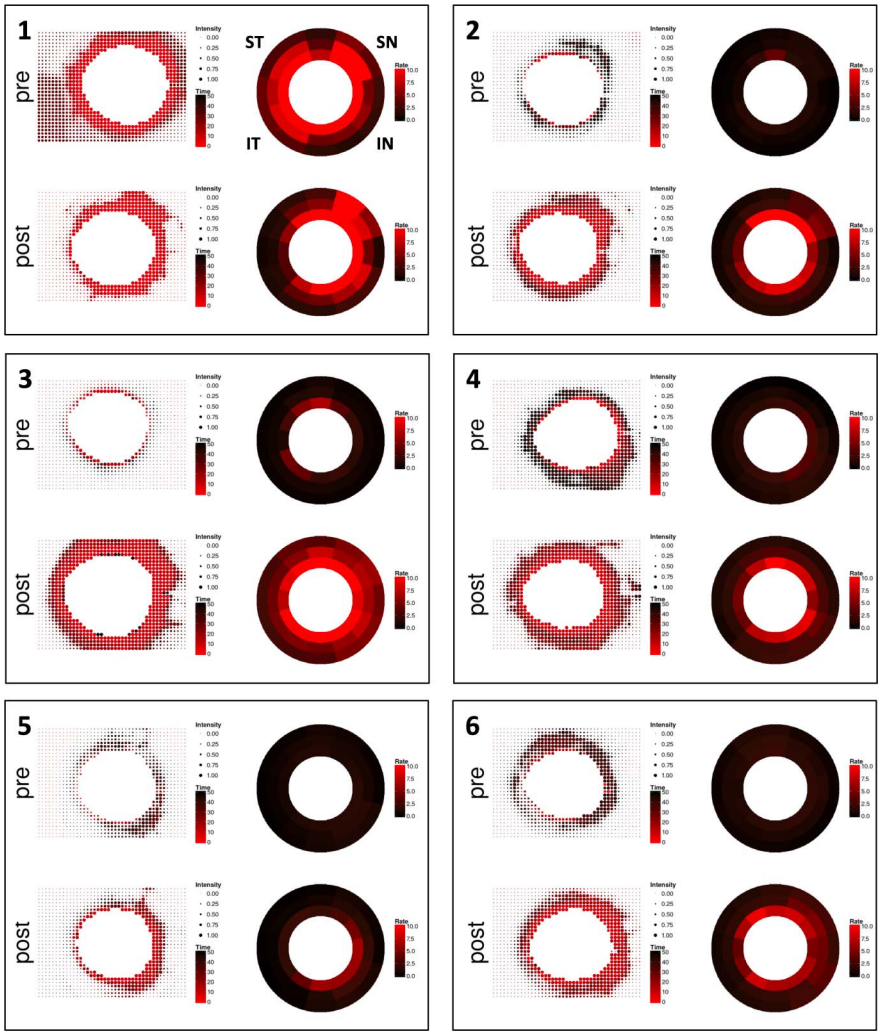

FIGURE 5. Quantitative canalograms with individual intensity fits (*left*) and circumferential flow rates (*right*). Both are increased in most eyes, even in quadrants away from the nasal AIT site.

peak intensity increased in the IN quadrant and in the SN quadrant, as well as in the remainder of the circumference (Fig. 6 left). In contrast, flow rate changes from pre- to post-AIT were more substantial in the nasal quadrants (Fig. 6B).

These changes from pre- to post-AIT were statistically significant in all quadrants but more pronounced in the IN and SN quadrants. Those quadrants remained significantly faster than the ST and IT quadrants. There was no difference between the ST and IT quadrants pre- or post-AIT.

DISCUSSION

Focal changes of conventional aqueous humor outflow are difficult to examine,[8,28] yet are crucial to better understand how elements downstream of the TM may influence outflow. There is ample new clinical evidence[29–33] that very significant outflow resistance exists downstream of the trabecular meshwork as trabecular ablation rarely achieves the theoretically lowest intraocular pressure, which would be equal to that of episcleral venous pressure according to the Goldmann equation.[1] The lack of an inexpensive, readily available, and high quality outflow model has impeded glaucoma research and training of surgery on this submillimeter structure alike. Here we address both with a differential canalography technique that allows examination of the effect of trabectome-mediated AIT on focal outflow in porcine eyes.

Visualization of the chamber angle and ablation of TM by AIT was quite similar to surgery in human patients. Angle surgery can be practiced in human eyes,[34] but costs of those are high and the corneal clarity is often too compromised to see the angle.[35] As a result, artificial eyes were preferred by

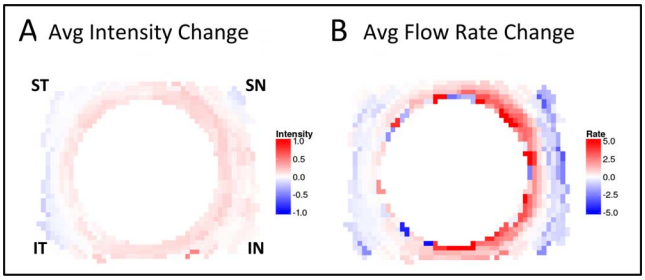

FIGURE 6. (A) Quantitative change analysis after AIT. Each eye produces a pair of images: change in fluorescence intensity (*left image*) and change in rate of fluorescence uptake (*right image*). *Red* (positive values) indicates greater intensity or rate of uptake following AIT; *blue* (negative values) indicates less intensity or reduced uptake. **(B)** Summarizing graph of intensity and rate change for all six eyes.

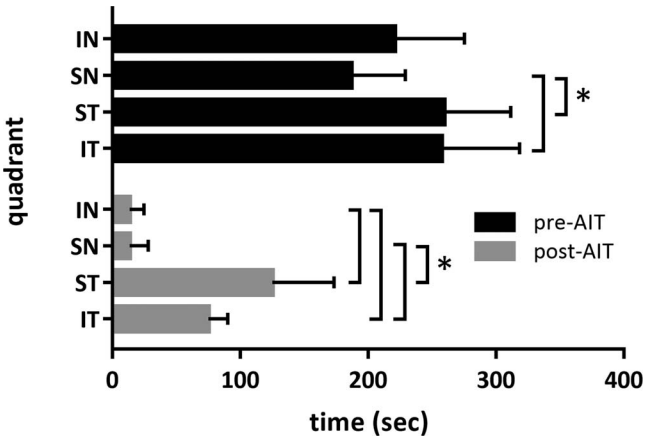

FIGURE 7. Outflow change summary after AIT. *Short bars* indicate fast filling not only in the nasal quadrants (IN and SN quadrant), but also in the temporal quadrants (ST and IT quadrants) following AIT.

trainees.[35] The histology following AIT shows that despite the anatomical differences between the pig and human chamber angle, an extensive ablation of TM can be achieved without an obvious coagulative thermal effect on adjacent tissues. Different from coagulation devices, the instrument used here generates plasma to ionize tissue and has a highly confined heat dissipation cone that is similar to photodisruptive lasers.[11]

The initial canalograms obtained with fluorescent microspheres demonstrated that TM must be removed before they can enter the conventional outflow system. As has been demonstrated before in human[6] and ungulate trabecular meshwork,[36] the size of 0.5 μm used here prevents spheres from moving into Schlemm's canal within the perfusion time used while preventing fluid blockage that can be observed with 10 μm spheres.[37] Our choice of relatively small beads had the advantage that smaller collector channels could be visualized.

Although the angular aqueous plexus of pigs does not have a continuous Schlemm's canal as primate eyes do, but rather multiple SC-like segments, we observed circumferential flow that extended far beyond the ablation site. This indicates that canal segments are connected and that supraphysiological flow from the site of ablated TM is displacing the normal flow that is still occurring through the nonablated TM.

The perilimbal flow analysis of differential canalograms showed high-flow areas near the IN and SN angle. In pig eyes, this matches the areas in between the recti muscles, where larger collector channels reside (Fig. 4).[17] The circumferential flow patterns observed here contradicts the assumption of noncontinuous SC segments in the pig. A three-dimensional reconstruction at a higher resolution than conventional histological sections by SD-OCT may be necessary. Such an approach has enabled discovery of previously overlooked valve-like elements in human eyes.[38,39]

We provide a heatmap summary image that combines fluorescence and flow rate of all six eyes. This allows us to visualize how flow can be enhanced in nonglaucomatous eyes to levels above the physiological flow rate and beyond the TM ablation area. In this constant pressure perfusion system, AIT led to increased flow and peak fluorescence in all quadrants, beyond the nasal site where AIT was performed. This has practical implications for patient care and suggests that it may not be necessary to obtain a very extensive ablation or circumferential access to the outflow tract. Carefully observing glaucoma surgeons have previously described fluid waves of saline displacing blood in collector channels after AIT.[40] These appeared to be limited to the site of ablation when observed through an operating microscope. Such visualization may relatively underestimate the amount of flow that could be detected with more sensitive, fluorescent dyes as used here.

There are well established angiography methods for organs larger than the anterior segment of the eye, such as the heart.[41] Characteristic for such angiography is that vessels branch off large primary vessels to subsequently smaller ones, and typically without collaterals.[42] The outflow tract of the eyes is different and has a much more diffuse and connected nexus of vessels with variable caliber.[7] The drainage system just distal to the outer wall of the SC is more similar to the honeycomb pattern of a capillary network,[7,43] but its vessels are larger and collapsible depending on the perfusion pressure.[44] This makes it challenging to use Doppler strategies to compute flow speeds in single vessels. The data presented here validate the use of fluorescence change[17] as a surrogate to tracking reflective particles.

In conclusion, we developed a method to quantify outflow enhancement from plasma-mediated AIT and show that nasal ablation of trabecular meshwork increased outflow not only locally but circumferentially. Methods and code provided here will aid further investigations into segmental outflow changes.

Acknowledgments

Supported by Grant K08EY022737 (NAL); the American Glaucoma Society (NAL); Grant P30-EY08099 (JSS); Research to Prevent Blindness (JSS); and Alpha Omega Alpha (HP).

Disclosure: **R.T. Loewen**, None; **E.N. Brown**, None; **G. Scott**, None; **H. Parikh**, None; **J.S. Schuman**, None; **N.A. Loewen**, Neomedix (R)

References

1. Brubaker RF. Goldmann's equation and clinical measures of aqueous dynamics. *Exp Eye Res*. 2004;78:633–637.
2. Nau CB, Malihi M, McLaren JW, Hodge DO, Sit AJ. Circadian variation of aqueous humor dynamics in older healthy adults. *Invest Ophthalmol Vis Sci*. 2013;54:7623–7629.
3. Yuan F, Schieber AT, Camras LJ, Harasymowycz PJ, Herndon LW, Allingham RR. Mathematical modeling of outflow facility increase with trabecular meshwork bypass and Schlemm canal dilation. *J Glaucoma*. 2016;25:355–364.
4. Hunter KS, Fjield T, Heitzmann H, Shandas R, Kahook MY. Characterization of micro-invasive trabecular bypass stents by ex vivo perfusion and computational flow modeling. *Clin Ophthalmol*. 2014;8:499–506.
5. de Kater AW, Melamed S, Epstein DL. Patterns of aqueous humor outflow in glaucomatous and nonglaucomatous human eyes. A tracer study using cationized ferritin. *Arch Ophthalmol*. 1989;107:572–576.
6. Hann CR, Fautsch MP. Preferential fluid flow in the human trabecular meshwork near collector channels. *Invest Ophthalmol Vis Sci*. 2009;50:1692–1697.
7. Francis AW, Kagemann L, Wollstein G, et al. Morphometric analysis of aqueous humor outflow structures with spectral-domain optical coherence tomography. *Invest Ophthalmol Vis Sci*. 2012;53:5198–5207.
8. Wang B, Kagemann L, Schuman JS, et al. Gold nanorods as a contrast agent for Doppler optical coherence tomography. *PLoS One*. 2014;9:e90690.
9. Gabriele Sandrian M, Wollstein G, Schuman JS, et al. Inflammatory response to intravitreal injection of gold nanorods. *Br J Ophthalmol*. 2012;96:1522–1529.

10. Rosenquist R, Epstein D, Melamed S, Johnson M, Grant WM. Outflow resistance of enucleated human eyes at two different perfusion pressures and different extents of trabeculotomy. *Curr Eye Res*. 1989;8:1233–1240.
11. Kaplowitz K, Schuman JS, Loewen NA. Techniques and outcomes of minimally invasive trabecular ablation and bypass surgery. *Br J Ophthalmol*. 2014;98:579–585.
12. Pfeiffer N, Garcia-Feijoo J, Martinez-de-la-Casa JM, et al. A randomized trial of a Schlemm's canal microstent with phacoemulsification for reducing intraocular pressure in open-angle glaucoma. *Ophthalmology*. 2015;1283–1293.
13. Wilmsmeyer S, Philippin H, Funk J. Excimer laser trabeculotomy: a new, minimally invasive procedure for patients with glaucoma. *Graefes Arch Clin Exp Ophthalmol*. 2006;244:670–676.
14. Mäepea O, Bill A. Pressures in the juxtacanalicular tissue and Schlemm's canal in monkeys. *Exp Eye Res*. 1992;54:879–883.
15. Malvankar-Mehta MS, Iordanous Y, Chen YN, et al. iStent with phacoemulsification versus phacoemulsification alone for patients with glaucoma and cataract: a meta-analysis. *PLoS One*. 2015;10:e0131770.
16. Kaplowitz K, Bussel II, Honkanen R, Schuman JS, Loewen NA. Review and meta-analysis of ab-interno trabeculectomy outcomes. *Br J Ophthalmol*. January 2016;100:594–600.
17. Loewen RT, Brown EN, Roy P, Schuman JS, Sigal IA, Loewen NA. Regionally discrete aqueous humor outflow quantification using fluorescein canalograms. *PLoS One*. 2016;11:e0151754.
18. Tripathi RC. Ultrastructure of the exit pathway of the aqueous in lower mammals: (A preliminary report on the "angular aqueous plexus"). *Exp Eye Res*. 1971;12:311–314.
19. Suárez T, Vecino E. Expression of endothelial leukocyte adhesion molecule 1 in the aqueous outflow pathway of porcine eyes with induced glaucoma. *Mol Vis*. 2006;12:1467–1472.
20. Groenen MAM, Archibald AL, Uenishi H, et al. Analyses of pig genomes provide insight into porcine demography and evolution. *Nature*. 2012;491:393–398.
21. Flicek P, Amode MR, Barrell D, et al. Ensembl 2014. Nucleic Acids Res. 2014;42:D749–D755.
22. Pairwise alignment human vs pig LastZ results. Ensembl. Available at: http://useast.ensembl.org/info/genome/compara/mlss.html?mlss=716. Accessed August 17, 2015.
23. McMenamin PG, Steptoe RJ. Normal anatomy of the aqueous humour outflow system in the domestic pig eye. *J Anat*. 1991;178:65–77.
24. Kaplowitz K, Loewen NA. Trabectome-mediated ab interno trabeculectomy for secondary glaucoma or as a secondary procedure. In: Aref AA, Varma R, eds. *Advanced Glaucoma Surgery. Essentials in Ophthalmology.* Cham, Switzerland: Springer International Publishing; 2015:15–29.
25. Loewen RT, Roy P, Park DB, et al. A porcine anterior segment perfusion and transduction model with direct visualization of the trabecular meshwork. *Invest Ophthalmol Vis Sci*. 2016;57:1338–1344.
26. Alford R, Simpson HM, Duberman J, et al. Toxicity of organic fluorophores used in molecular imaging: literature review. *Mol Imaging*. 2009;8:341–354.
27. R: The R Project for Statistical Computing. Available at: http://www.r-project.org/. Accessed June 15, 2015.
28. Cha EDK, Xu J, Gong L, Gong H. Variations in active outflow along the trabecular outflow pathway. *Exp Eye Res*. 2016;ppii:s0014–4835
29. Neiweem AE. Bussel II, Schuman JS, Brown EN, Loewen NA. Glaucoma surgery calculator: limited additive effect of phacoemulsification on intraocular pressure in ab interno trabeculectomy. *PLoS One*. 2016;11:e0153585.
30. Parikh HA, Bussel II, Schuman JS, Brown EN, Loewen NA. Coarsened exact matching of phaco-trabectome to trabectome in phakic patients: lack of additional pressure reduction from phacoemulsification. *PLoS One*. 2016;11:e0149384.
31. Loewen RT, Roy P, Parikh HA, Dang Y, Schuman JS, Loewen NA. Impact of a glaucoma severity index on results of trabectome surgery: larger pressure reduction in more severe glaucoma. *PLoS One*. 2016;11:e0151926.
32. Bussel II, Kaplowitz K, Schuman JS, Loewen NA; Trabectome Study Group. Outcomes of ab interno trabeculectomy with the trabectome by degree of angle opening. *Br J Ophthalmol*. 2015;99:914–919.
33. Bussel II, Kaplowitz K, Schuman JS, Loewen NA, Group TS; Trabectome Study Group. Outcomes of ab interno trabeculectomy with the trabectome after failed trabeculectomy. *Br J Ophthalmol*. 2014;99:258–262.
34. Patel SP, Sit AJ. A practice model for trabecular meshwork surgery. *Arch Ophthalmol*. 2009;127:311–313.
35. Patel HI, Levin AV. Developing a model system for teaching goniotomy. *Ophthalmology*. 2005;112:968–973.
36. Johnson M, Johnson DH, Kamm RD, DeKater AW, Epstein DL. The filtration characteristics of the aqueous outflow system. *Exp Eye Res*. 1990;50:407–418.
37. Weber AJ, Zelenak D. Experimental glaucoma in the primate induced by latex microspheres. *J Neurosci Methods*. 2001;111:39–48.
38. Johnstone MA, Saheb H, Ahmed IIK, Samuelson TW, Schieber AT, Toris CB. Effects of a Schlemm canal scaffold on collector channel ostia in human anterior segments. *Exp Eye Res*. 2014;119:70–76.
39. Li P, Johnstone M, Wang RK. Full anterior segment biometry with extended imaging range spectral domain optical coherence tomography at 1340 nm. *J Biomed Opt*. 2014;19:046013.
40. Fellman RL, Grover DS. Episcleral venous fluid wave: intraoperative evidence for patency of the conventional outflow system. *J Glaucoma*. 2012;23:347–350.
41. Chung W-Y, Choi B-J, Lim S-H, et al. Three dimensional quantitative coronary angiography can detect reliably ischemic coronary lesions based on fractional flow reserve. *J Korean Med Sci*. 2015;30:716–724.
42. Gómez-Menchero AE, Díaz JF, Sánchez-González C, et al. Comparison of dual-axis rotational coronary angiography (XPERSWING) versus conventional technique in routine practice. *Rev Esp Cardiol (Engl Ed)*. 2012;65:434–439.
43. Gong H, Francis A. Schlemm's canal and collector channels as therapeutic targets. In: Samples JR, Ahmed IIK, eds. *Surgical Innovations in Glaucoma*. New York, NY: Springer; 2014:3–25.
44. Hann CR, Vercnocke AJ, Bentley MD, Jorgensen SM, Fautsch MP. Anatomic changes in Schlemm's canal and collector channels in normal and primary open-angle glaucoma eyes using low and high perfusion pressures. *Invest Ophthalmol Vis Sci*. 2014;55:5834–5841.

Investigative Ophthalmology & Visual Science